Heliyon 6 (2020) e03602

Contents lists available at ScienceDirect

Heliyon

journal homepage: www.cell.com/heliyon

Research article

Low-cost fabrication of optical tissue phantoms for use in biomedical imaging

Lindokuhle Ntombela, Bamise Adeleye, Naven Chetty *

School of Chemistry and Physics, University of KwaZulu–Natal, Private Bag X01, Scottsville, 3209, South Africa

ARTICLE INFO

Keywords:
Medical imaging
Optics
Agar
Phantoms tissues
Al2O3 particles
Optical properties

ABSTRACT

The rapid development of new optical imaging techniques is dependent on the availability of low-cost and easily reproducible standards for technique validation. This work describes a low-cost fabrication process of an agar gel-based phantom that may accurately simulate the optical properties of different human tissues at 532 and 630nm wavelengths. It was designed to match the optical properties of the brain, bladder wall, and lung tissues. These low-cost phantoms use agar powders dissolved in water as the bulk matrix. The latter is loaded with varying amounts of India ink, and aluminium oxide Al_2O_3 particles for optical absorption and scattering targets. The optical properties (absorption and scattering coefficients), the primary design factor and critical parameters of these phantoms were deduced from measurements of the total attenuation coefficients (μ_t).

It is anticipated that the constructed tissue phantoms have the potential to be used as a reference standard since it's possible to preserve the optical properties in a period exceeding two years, under ideal storage conditions.

1. Introduction

Optical tissue phantoms are necessary for the development and standardization of bio-optical techniques and calibration of steady-state optical measurements on real tissues to establish quantitative information before clinical trials [1, 2, 3]. They play an important role in understanding the optical characteristics of biological tissues and the description of light propagation through them [4, 5]. However, recent technological advancement from prototyping to clinical testing for improvement in imaging techniques requires the development of a standardized and reproducible protocol for phantom fabrication to validate these techniques and minimize variation in phantom optical properties with time [1, 6].

A major challenge in phantom tissue fabrication is the high cost and the laborious nature of the methodologies proposed for their development [3]. Furthermore, the easy degradation and low temporal stability of commonly used phantom materials often lead to a limitation in the specificity of the heterogeneities or complex, layered structures of the biological tissues to be mimicked [3, 7]. The related alterations in optical properties from individual tissue structures and conditions such as oxygen saturation, the volume of blood, water content as well as the age of the person might also be significant factors [8].

This led to the use of the polymeric material Agar, a dry powder comprising of seaweed polysaccharides in this work. Agar is particularly chosen for its ability to form stable matrices that allow for the inclusion of various entities to simulate both optical and biochemical properties of phantom tissue similar to those of biological tissue. Further, it allows for the tunability of absorption and scattering characteristics [9, 10].

Nevertheless, the existence of a standardized Agar gel phantom fabrication procedure mimicking various human tissues in a range of wavelengths typically required for more specialised applications is of great interest to ensure that their production depends at the minimum on handling [11, 12]. To date, several efforts have been made to describe the preparation recipes for tissue-mimicking agar phantoms. Jung et al. [13] constructed an Agar phantom with size 300 × 300 × 200 mm to mimic the lower abdomen of a human body and suitable to measure the temperature distribution characteristics of a radiofrequency hyperthermia device. It was prepared by mixing 100 ml CAR-15 Agar powder and 19, 000 ml distilled water. The phantom effectively determines the temperature distribution of the hyperthermia device. Wagnières et al. [14] attempted to obtain a phantom with optical properties corresponding to the human oesophageal wall within the visible light range. They added various amounts of silicon dioxide, Intralipid, ink and concentrated blood to an agarose matrix. Fluorochromes were used to simulate tissue containing an exogenous fluorescent marker, and since most fluorochromes

* Corresponding author.
E-mail address: chettyn3@ukzn.ac.za (N. Chetty).

https://doi.org/10.1016/j.heliyon.2020.e03602
Received 1 July 2019; Received in revised form 28 October 2019; Accepted 11 March 2020
2405-8440/© 2020 Published by Elsevier Ltd. This is an open access article under the CC BY-NC-ND license (http://creativecommons.org/licenses/by-nc-nd/4.0/).

used in cancer photodynamic therapy and photo-detection have an affinity for proteins, bovine serum was used to introduce protein into the phantoms.

Although the optical properties of the serum do not play a significant role in the overall optical coefficients of the phantoms, the main limitation of this approach was the probable variations in optical properties due to the imperfect reproducibility of the preparation process.

Mustari et al. [15] in their work described the fabrication of tissue-mimicking optical phantoms for use in diffuse reflectance spectroscopy and multispectral imaging. A coffee solution and lipid emulsion were added to an agarose matrix. The phantom produced successfully represents the diffuse reflectance spectra of living tissues. However, obtaining subsequent phantom with similar optical properties is difficult to achieve due to the need to maintain a temperature range for the base material.

Vulcanized Polydimethylsiloxane (PDMS) tissue phantoms tuned to specific optical properties in the near-infrared spectrum were fabricated for system calibration and performance testing [16]. Scattering and absorption properties were set by titanium dioxide (TiO_2) and India ink (PRO-4100, Pro Art). A curing agent was manually mixed with the TiO_2 in an ultrasonic bath for 30 min followed by the addition of bulk PDMS and India ink suspension. The solution was further hand-mixed for 15minutes and poured into a mould (softball display case) for curing. Compared to gelatin-based phantoms, the cured PDMS phantoms are easier to transport with a longer usable life.

A similar study by Jang et al. [17] fabricated stable Solid Haemoglobin-Polymer (SHP) materials with haemoglobin spectral absorption properties above 450–1000 nm. Fully oxygenated human haemoglobin solution with normal concentration level (150 g/l) was mixed with PDMS the base matrix material using a sonicator.

A PDMS curing agent (hardener) was added to the homogeneous mixture at a mass ratio (PDMS: hardener) of 10:1 and stirred for 5 min until uniform. Phantoms of various thicknesses were produced using an aluminium-disk PMDS mould placed in a vacuum chamber for about 1 h to extract created bubbles. Although PDMS is capable of rapid curing at higher temperatures, their process required room-temperature curing for 1–2 days to avoid thermal effects such as denaturation on haemoglobin.

Moffitt et al. [18] described a method of preparing solid phantoms simulating the optical properties of biological tissues at 690 and 830nm. The phantoms consist of three components: a two-part polyurethane system, absorbing chromophores (phthalocyanine and palladium dye) at 690 and 830nm, and scattering agents (Titanium dioxide TiO_2). Stock solutions in xylene of the two powdered dyes and TiO_2 in ethanol were diluted into each part of the polyurethane systems. All samples were mixed and poured into cuvettes of path length 1 cm for casting. Degassing was done by placing the samples in a desiccator/vacuum chamber following which the phantoms were covered and left on a level surface. The phantoms produced were solid but the polyurethane was relatively soft at 24 h.

The irregular readings of tissue oxygen haemoglobin saturation (StO_2) by different near-infrared spectroscopy (NIRS) oximeters led Kleiser et al. [19] to perform simultaneous measurements on liquid phantom mimicking the optical properties of neonatal heads.

The phantom consisted of phosphate-buffered saline (PBS) to which 74 ml IL (20 %) and defined amounts of human blood from expired human erythrocyte concentrate bags including Sodium bicarbonate buffer (SBB) were added. Fresh baker yeast was added when required, for haemoglobin deoxygenation. The phantom was though re-oxygenated by pure oxygen (O_2) through bubbling which could have created an inhomogeneity.

In this study, we present a detail low-cost but simple fabrication technique of Agar-gels based optical phantoms suitable for applications in the green (532 nm) and red (630 nm) He–Ne laser wavelength, and further characterize their optical properties to identify the phantom geometry and optical agents that could successfully mimic the target tissue as an alternative to commonly used costly models of pre-clinical evaluation. Specifically, the phantoms have been designed to replicate the optical properties identical to the human brain grey matter, bladder wall, and lung tissues.

The developed phantoms are convenient for realistic evaluation before validation by real tissues since they consist of carefully measured concentrations of the scattering and absorbing agents needed to provide the intrinsic optical properties of the simulated tissue.

2. Materials and methods

2.1. Materials selection

The Tryptone soy and Bacteriological Agar powder (Sigma Aldrich, MO, USA) were the phantom base materials for this study. Agar based gels, in addition to their hardening qualities, are considered inexpensive, easy to produce, have negligible absorption, non-toxic and durable at high temperatures [10]. It can remain stable up to two and a half years under ideal storage conditions [10, 20]. Additionally, the relaxation time of the Agar gel is similar to that of human tissue (40–150 ms) and can be varied to simulate different tissue values [21].

Phantom optical properties were controlled by introducing varying concentrations of Aluminium oxide (Al_2O_3) particles (64271, Darmstadt, Germany) and India ink (PRO-4100, Pro Art) as the scattering and absorbing agents, respectively. The choice of optical agents was driven by their stability in the basic medium. They have also been used extensively in other visible wavelength phantoms.

The amounts of primary components utilized were determined with a digital balance (readability of 0.01 g) capable of accurately measuring the relatively small masses of the materials used in the study.

2.2. Phantom recipes and fabrication methods

All tissue phantoms samples were prepared by dissolving a certain amount by weight of the Agar (Bacteriological or Soy) powder and adding varying concentrations of India ink and aluminium oxide (Al_2O_3) that approximate the desired optical properties for the biological tissue of interest at the imaging wavelength(s) in 100 ml of deionized water. The phantom recipes, together with the mimicked tissue types for each base material and laser wavelength are listed in Table 1.

The solution was placed on a hot plate and heated to approximately 94 °C the temperature at which the agar activates while stirring continuously to allow for all granules of agar powder and scattering particles to dissolve thus creating a firm gel. The temperature of the sample during the heating process was monitored using a Techgear TG732TK dual channel digital thermometer modified to utilize a thermocouple attached on the reverse side of a Velcro strap. The digital thermocouple strapped around the beaker provides accurate temperature measurements of the heated solution with a stated accuracy of ±5 °C.

The fabricated optical phantom sample was then allowed to cool to 20 °C and wrapped with aluminium foil (to preserve the sample from draining and unwanted particles) before storing for at least 24 h in a refrigerator to solidify. The complexity of the preparation process, especially the varying concentrations of added optical agents is dependent on the base material and the intended quality of the resulting gel.

2.3. Optical properties measurements

2.3.1. Experimental set-up

In line with the low-cost concept of this study, the optical behaviour of each phantom tissue was evaluated by using the set up shown in Figure 1. Phantoms samples of various thicknesses were irradiated with either a green or red He–Ne laser light of wavelength 532 and 630 nm respectively. The laser beam kept at a constant distance away from the sample was first split into a reference and sample beam by a 25 mm diameter cube beam splitter (Edmund Optics, USA), to continuously monitor the incident beam power.

Table 1. Phantom recipes together with the mimicked tissue types for each base material.

Base material	Phantom recipe	Laser wavelengths	Mimicked tissue
Bacteriological Powder	2.0g of Agar powder, 0.3 g Al_2O_3 + 0.3 ml India Ink	532 nm	Brain
	2.0g of Agar powder, 0.5 g Al_2O_3 + 0.5 ml India Ink	532 nm	Bladder
	2.0g of Agar powder, 0.1 g Al_2O_3 + 0.1 ml India Ink	630 nm	Lungs
Soy Powder	6.0g of Agar powder, 0.3 g Al_2O_3 + 0.3 ml India Ink	532 nm	Brain
	6.0g of Agar powder, 0.5 g Al_2O_3 + 0.5 ml India Ink	532 nm	Bladder
	6.0g of Agar powder, 0.1 g Al_2O_3 + 0.1 ml India Ink	630 nm	Lungs

The collimated incident and transmitted light intensity through the samples were measured using an EO 54-018 digital handheld laser power meter (detector) with aperture size 8 mm (Edmund Optics, USA), positioned behind the sample holder. The tissue phantoms were placed on a 1mm thick glass slide inside a sample holder located at a distance of about 0.6m from the beam splitter.

The absorption and scattering coefficients of the created tissue phantoms were determined following the Beer-Lambert law relationship Eq. (1). Assuming multiple scattering does not take place and that the scattering is caused by the added Al_2O_3 particles [22]:

$$\frac{P}{P_o} = e^{-\mu_t d} \tag{1}$$

where P is the measured light intensity at the detector at a certain sample thickness d, P_o is the intensity of incident length and μ_t is the total attenuation coefficient.

The total attenuation coefficient is represented by the slope of the linear curve on an $\ln\left[P/P_o\right]$ versus thickness graph, given by Eq. (2)

$$\mu_t = -\frac{1}{d}\ln\left[\frac{P}{P_o}\right] \tag{2}$$

In turbid samples, the total attenuation coefficient μ_t is also described as the sum of absorption μ_a and scattering μ_s coefficient [13], as expressed in Eq. (3),

$$\mu_t = \mu_a + \mu_s \tag{3}$$

The refractive index n of the phantoms was also ascertained using the method introduced by Li et al. [23] based on total internal reflection.

2.3.2. Determination of absorption and scattering coefficients

To determine the optical properties for each tissue phantom, Agar phantom samples mixed with different concentrations of Al_2O_3 particles were first fabricated and sliced into six different thicknesses (Tables 2, 3, 4, 5, 6, and 7) to measure the scattering coefficients with the assumption that ($\mu_t \approx \mu_s$). Subsequently, the desired tissues were simulated by adding a concentration of India ink to the same amount of Al_2O_3 particles and Agar powder. The absorption coefficient μ_a was determined from the total attenuation coefficient μ_t following Eq. (3).

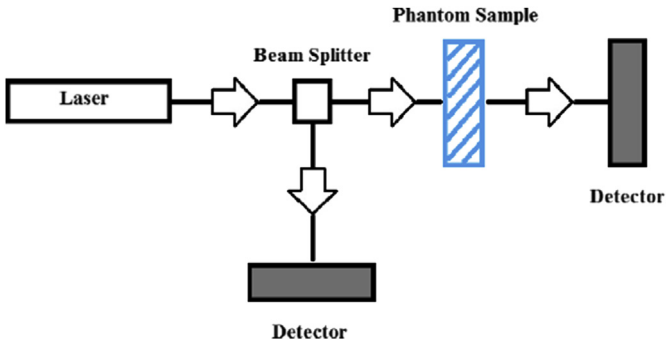

Figure 1. Schematic illustration of the procedure involved in laser irradiation of phantom samples.

Table 2. The power intensities of the 532 nm laser through different thicknesses of the brain bacteriological Agar phantoms.

Sample Thickness (mm)	Incident Power (mW)	Transmitted Power (mW)	$-\ln P/P_o$
2.66	55.47	31.67	0.560
4.71	54.37	26.57	0.716
6.80	53.97	20.97	0.945
8.56	53.37	15.87	1.213
10.66	55.37	12.77	1.467
12.84	53.97	8.17	1.888

2.4. Results and discussion

Figure 2a and 2b show the microscopic characterization of the Aluminium oxide (Al_2O_3) particles performed with a JOEL JEM-1400

Table 3. The power intensities of the 532nm laser through different thicknesses of the bladder bacteriological Agar phantoms.

Sample Thickness (mm)	Incident Power (mW)	Transmitted Power (mW)	$-\ln P/P_o$
2.94	52.37	27.42	0.647
4.56	52.77	23.36	0.815
6.15	54.87	19.38	1.041
8.24	54.77	14.40	1.336
10.16	55.89	10.03	1.718
12.65	52.67	5.48	2.263

Table 4. The power intensities of the 630 nm laser through different thicknesses of the lung bacteriological Agar phantoms.

Sample Thickness (mm)	Incident Power (mW)	Transmitted Power (mW)	$-\ln P/P_o$
2.91	7.57	3.97	0.645
4.78	7.61	3.26	0.848
6.44	7.65	2.41	1.155
8.14	7.51	1.79	1.434
10.46	7.59	1.19	1.853
12.81	7.58	0.77	2.287

Table 5. The power intensities of the 532 nm laser through different thicknesses of the brain soy Agar phantoms.

Sample Thickness (mm)	Incident Power (mW)	Transmitted Power (mW)	$-\ln P/P_o$
2.95	53.07	23.53	0.732
4.96	54.67	21.77	0.921
6.35	54.87	17.61	1.136
8.18	54.37	13.26	1.411
10.27	54.44	9.31	1.766
12.86	54.27	5.34	2.319

Table 6. The power intensities of the 532 nm laser through different thicknesses of the bladder soy Agar phantoms.

Sample Thickness (mm)	Incident Power (mW)	Transmitted Power (mW)	$-\ln P/P_o$
2.85	51.27	23.77	0.769
4.89	53.27	19.87	0.986
6.13	53.27	15.57	1.230
8.17	54.97	11.05	1.604
10.25	54.77	6.93	2.607
12.29	51.17	3.91	2.572

transmission electron microscope (Joel Ltd., Tokyo, Japan), fitted with a GATAN Orius camera. The Al_2O_3 displayed spherical shaped particles with an average size between 30-65 nm closely matching the manufacturer specification. The diffraction pattern showed no evidence of the presence of amorphous phases in the aluminium oxides indicating its crystalline nature.

Figures 3 and 4 show the graph of $\ln\left[P/P_o\right]$ plotted as a function of thickness for all phantom samples types with the error bar plots showing the standard deviation for each phantom. The slope of the least-squares line fits perform on the data sets gives the total attenuation coefficient μ_t, from which the optical properties are evaluated based on the hypothesis that the absorption μ_a of the India ink and the scattering coefficient μ_s of the Agar act additionally to create the μ_t of the phantom according to Eq. (3). Linear regression analysis was carried out for comparison of total attenuation coefficient μ_t values for different phantoms tissues on the basis of base materials.

No statistically significant differences were found between the values for the brain ($F = 5.140$, $P > 0.05$), bladder ($F = 2.832$, $P > 0.05$) and lungs ($F = 5.052$, $P > 0.05$) tissue respectively. Moreover, a very strong correlation (R^2) value of 0.9 was found between related tissues with the bacteriological and soy Agar materials, showing a positive relationship exists between the phantoms tissues.

The optical properties of the fabricated tissue phantoms at the wavelength of interest for each base material are shown in Tables 8 and 9. The values obtained were compared to previously published data at 532 and 630 nm in the literature (Table 10) [24].

Table 7. The power intensities of the 630 nm laser through different thicknesses of the lung soy Agar phantoms.

Sample Thickness (mm)	Incident Power (mW)	Transmitted Power (mW)	$-\ln P/P_o$
2.98	7.15	3.41	0.740
4.96	7.57	2.79	0.998
6.22	7.61	2.18	1.250
8.26	7.71	1.47	1.657
10.23	7.49	1.01	2.004
12.35	7.42	0.59	2.532

Specifically, the optical coefficients (μ_a, μ_s) of the Agar gel phantoms were found to be in agreement with data reported by Yaroslavsky et al. [25] and Beck et al. [26] for the human brain grey matter and bladder wall tissues at 532 nm, and by Beek et al. [27] for a deflated oxygenated lung at 630 nm respectively.

The optical properties are dependent on the wavelength of interest, the base material, and the concentrations of the particles within the phantom [28]. In particular, the rate of absorption was nearly identical, indicating the scattering effect of the pure Agar phantoms to be minor over the wavelength range. However, the scattering coefficient of Al_2O_3 in each phantom type was found to differ by approximately 0.3 for the same amount of Agar powder with an identical wavelength.

To evaluate the temporal stability of the fabricated phantoms, samples were randomly selected for each phantom tissue, wrapped up and stored in a refrigerator. Degradation was defined as a loss in texture and

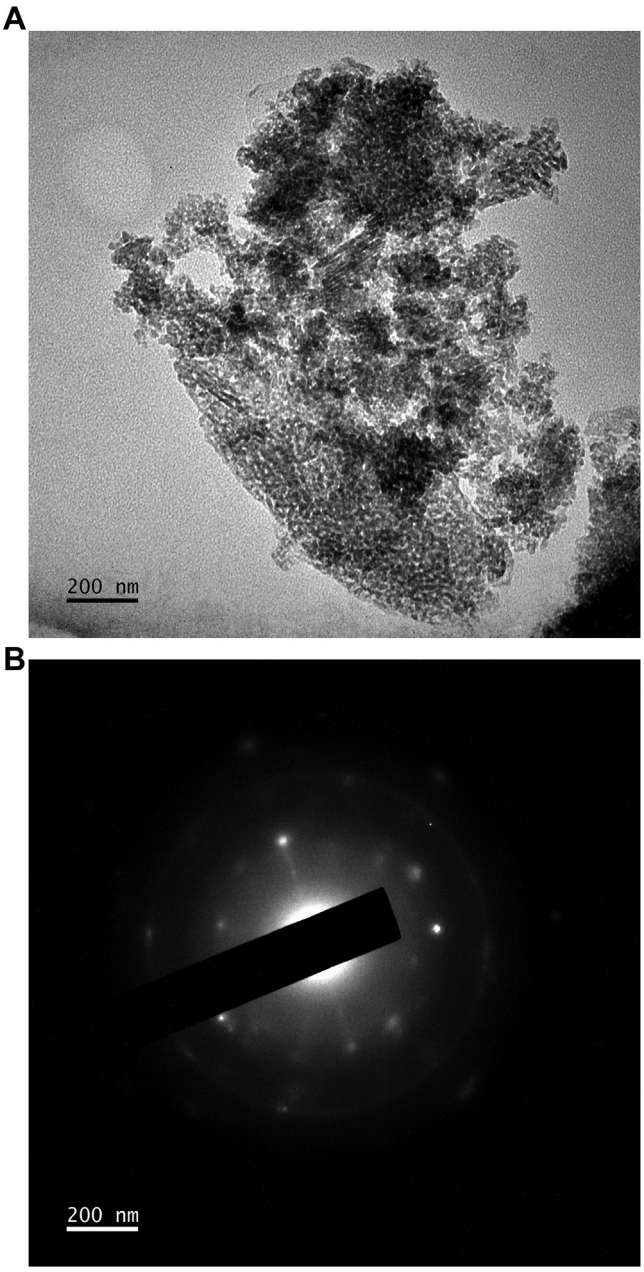

Figure 2. (a) Transmission electron micrographs, 40k magnification; with (b) the diffraction pattern showing the crystalline nature of the aluminium oxides (Al_2O_3) particles.

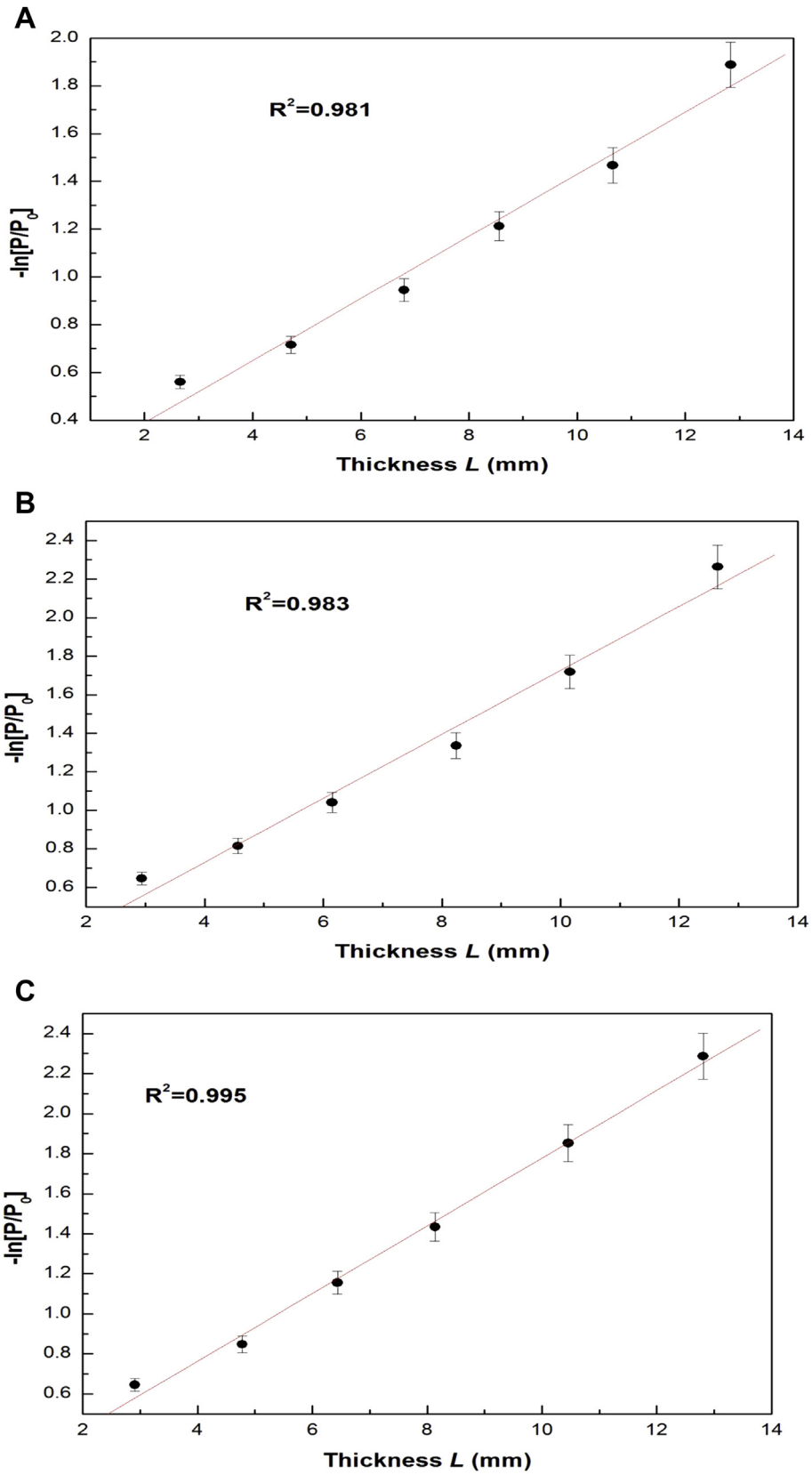

Figure 3. The logarithmic intensity as a function of thickness with associated linear fitting options to determine the total attenuation coefficients for the bacteriological Agar phantoms (A) Brain, (B) Bladder and (C) Lungs at 532, 532 and 630nm respectively.

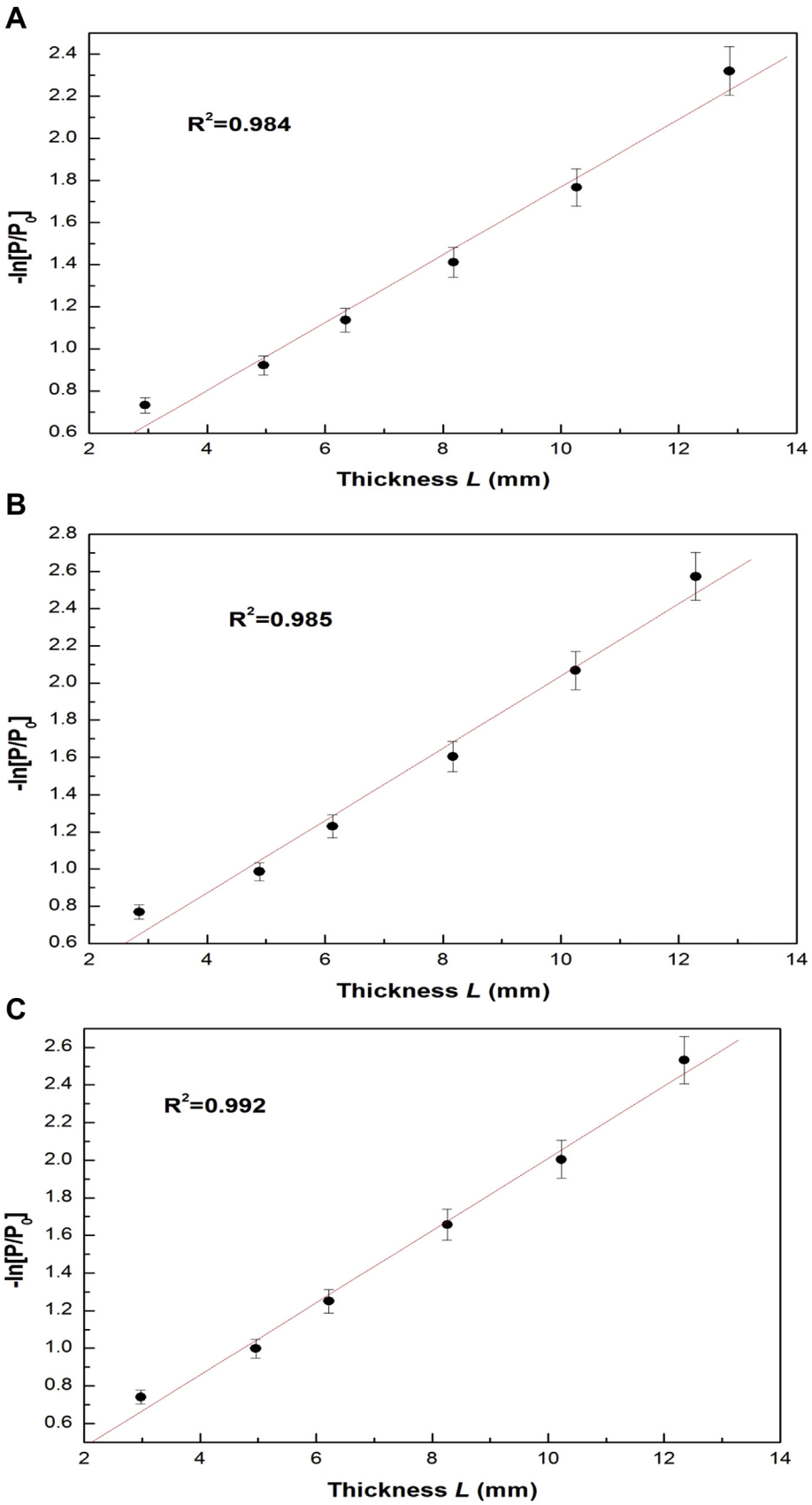

Figure 4. The logarithmic intensity as a function of thickness with associated linear fitting options to determine the total attenuation coefficients for the Soy Agar phantoms (A) Brain, (B) Bladder and (C) Lungs at 532, 532 and 630nm respectively.

Table 8. Optical properties of bacteriological Agar tissue-like phantoms.

wavelength (nm)	$\mu_a(cm^{-1})$	$\mu_s(cm^{-1})$	refractive Index
532	0.481 ± 0.026	0.819 ± 0.066	1.334
532	0.352 ± 0.050	1.308 ± 0.059	1.334
630	0.323 ± 0.557	1.368 ± 0.025	1.335

Table 9. Optical properties of the Soy Agar tissue-like phantoms.

wavelength (nm)	$\mu_a(cm^{-1})$	$\mu_s(cm^{-1})$	refractive Index
532	0.536 ± 0.116	1.110 ± 0.063	1.339
532	0.307 ± 0.002	1.604 ± 0.110	1.340
630	0.502 ± 0.061	1.417 ± 0.024	1.337

appearance. There was no notable change in refrigerated samples following two to three weeks of production in contrast to the slight desiccation observed in the unrefrigerated samples after a week. However, with the addition of antifungal agents, agar phantom can maintain stable optical properties for periods over two years [29].

Moreover, to assess the repeatability of the fabrication process, the measurement of the optical properties was performed for phantoms reproduced using our proposed method. In this instance, measurements were made for five differing thickness of each phantom with values of $\mu_a = 0.476 \pm 0.024\ cm^{-1}$ and $\mu_s = 0.815 \pm 0.057\ cm^{-1}$ at 532 nm, $\mu_a = 0.351 \pm 0.046\ cm^{-1}$ and $\mu_s = 1.294 \pm 0.031\ cm^{-1}$ at 532 nm, $\mu_a = 0.316 \pm 0.544\ cm^{-1}$ and $\mu_s = 1.366 \pm 0.019\ cm^{-1}$ at 630 nm for the bacteriological Agar brain, bladder and lung tissue phantoms. The corresponding optical coefficients for the Soy Agar phantoms were $\mu_a = 0.540 \pm 0.09\ cm^{-1}$ and $\mu_s = 1.111 \pm 0.053\ cm^{-1}$ at 532 nm, $\mu_a = 0.308 \pm 0.001\ cm^{-1}$ and $\mu_s = 1.606 \pm 0.104\ cm^{-1}$ at 532 nm, and $\mu_a = 0.497 \pm 0.049\ cm^{-1}$ and $\mu_s = 1.415 \pm 0.021\ cm^{-1}$ at 630 nm. These values are in close approximation to the optical properties of desired tissues with observed differences within experimental variability.

There were slight differences in the determined optical properties in comparison to values published for various agar-based phantoms. Cho et al. [30] reported an absorption coefficient of 0.24 cm^{-1} for skin and 0.52 cm^{-1} for fat tissue while in another study by Iizuka et al. [31] values of 0.50 ± 0.04 and 0.7 ± 0.1 cm^{-1} for unspecified tissue samples was given. This demonstrates the concentrations and different constituents of the fabricated phantoms, which are decisive factors for their optical properties [14, 31].

The optical properties depend on the biological variation of the tissues and the values can present significant variations due to measuring techniques, light propagation models and preparation techniques [32, 33].

The published approximate range of property values determined for various tissue types is nonetheless a great aid to those developing novel optical devices or planning therapeutic protocols [8].

There are a few sources of errors in this study. It is evident that the fitted straight-lines from Figures 3 and 4 do not pass through the origin as expected. However, this does not influence the total attenuation coefficient considering it's determined from the slope only [34]. Secondly, the optical properties were evaluated following the additive law of optical coefficients. The validity of the law has been tested by comparison with experimentally predicted optical coefficients, resulting in differences of less than 5% [35].

Another source of uncertainty is in the measurement of the refractive indices n values, due to complexities and variation in tissue samples with about 0.4% maximum experimental error in reasonable agreement with literature.

Finally, the phantoms were fabricated under the assumption that neither the Al_2O_3 particles nor India ink absorbs or scatter light at this wavelength. The induced effect is nevertheless negligible in the visible light spectrum [14].

Table 10. In-vivo optical properties of tissues.

Tissue	wavelength (nm)	$\mu_a(cm^{-1})$	$\mu_a(cm^{-1})$
Brain	532	0.02–3.84	0.10–46.3
Bladder	532	0.27–0.71	1.28–3.30
Lung	630	0.16–1.36	1.07–83.81

2.5. Conclusion

We have demonstrated the possibility of fabricating optical tissue phantoms with desired optical properties using an inexpensive and easy to follow procedure. The method proposed enables the creation of an Agar-based phantom that may accurately simulate the optical properties of the human brain, bladder and lung tissues at selected wavelengths. With further refinement these phantoms could be very useful in photo-medicine studies, for instance, predicting and optimizing response to photo-thermal therapies.

A unique advantage of the obtained results is that the optical parameters are reproducible since the homogeneity of the phantoms could be confirmed and the preparation and measurement procedure was similar for all phantoms. Furthermore, multilayer fabrication is possible by stacking several slices of prepared samples using water as an optical coupler to simulate complex structures.

Declarations

Author contribution statement

Lindokuhle Ntombela: Performed the experiments; Analyzed and interpreted the data.

Bamise Adeleye: Analyzed and interpreted the data; Wrote the paper.

Naven Chetty: Conceived and designed the experiments; Contributed reagents, materials, analysis tools or data; Wrote the paper.

Funding statement

This work was supported by the University of KwaZulu-Natal, South Africa.

Competing interest statement

The authors declare no conflict of interest.

Additional information

No additional information is available for this paper.

References

[1] J.P. Bouchard, I. Noiseux, I. Veilleux, O. Mermut, The role of optical tissue phantom in verification and validation of medical imaging devices, Int. Workshop Biophot. (2011) 1–3.

[2] R. Srinivasan, D. Kumar, M. Singh, Optical tissue-equivalent phantoms for medical imaging, Trends Biomater. Artif. Organs 15 (2) (2002) 42–47.

[3] L. Hernandez-Quintanar, M. Rodriguez-Salvador, Discovering new 3D bioprinting applications: analysing the case of optical tissue phantoms, Int. J. Bioprint 5 (1) (2019) 178.

[4] B.W. Pogue, M.S. Patterson, Review of tissue simulating phantoms for optical spectroscopy, imaging, and dosimetry, J. Biomed. Optic. 11 (4) (2006), 041102.

[5] J. Gwamuri, A.V. Gholap, T.S.M. Shartir, P.K. Bassuah, Investigating light propagation in turbid media by evaluating optical properties of phantom tissues, in: Proc. from the 2nd International Conference on Appropriate Technology, Bulawayo, Zimbabwe, 2006. July 12- 15.

[6] D. Wang, Y. Chen, J.T.C. Liu, "A liquid optical phantom with tissue-like heterogeneities for confocal microscopy," Biomed, Optic Express 3 (12) (2012) 3153–3160.

[7] L.C. Cabrelli, P.I. Pelissari, A.M. Deana, A.A. Carneiro, T.Z. Pavan, Stable phantom materials for ultrasound and optical imaging, Phys. Med. Biol. 62 (2) (2017) 432–447.
[8] S.L. Jacques, Optical properties of biological tissues: a review, Phys. Med. Biol. 58 (11) (2013) R37–R61.
[9] G. Lamouche, B.F. Kennedy, K.M. Kennedy, C.E. Bisaillon, A. Curatolo, G. Campbell, V. Pazos, D.D. Sampson, Review of tissue simulating phantoms with controllable optical, mechanical and structural properties for use in optical coherence tomography, Biomed. Optic Express 3 (6) (2012) 1381–1398.
[10] G. Menikou, C. Damianou, Acoustic and thermal characterization of agar-based phantoms used for evaluating focused ultrasound exposures, J. Ther. Ultrasound 5 (2017) 1–14.
[11] R.A. O Jaime, R.L.Q. Basto, B. Lamien, H.R.B. Orlande, S. Eibner, O. Fudym, Fabrication methods of phantoms simulating optical and thermal properties, Procedia Eng. 59 (2013) 30–36.
[12] M.O. Culjat, D. Goldenberg, P. Tewari, R.S. Singh, A review of tissue substitutes for ultrasound imaging, Ultrasound Med. Biol. 36 (2010) 861–873.
[13] D.K. Jung, S.K. Kim, J.H. Lee, S.M. Youn, H.D. Kim, S.A. Oh, J.W. Park, J.W. Yea, Comparison of temperature distribution in agar phantom and gel bolus phantom by radiofrequency hyperthermia, Prog. Med. Phys. 27 (4) (2016).
[14] G. Wagnières, S. Cheng, M. Zellweger, N. Utke, D. Braichotte, J.P. Ballini, H. van den Bergh, An optical phantom with tissue-like properties in the visible for use in PDT and fluorescence spectroscopy, Phys. Med. Biol. 42 (1997) 1415–1426.
[15] A. Mustari, I. Nishidate, M.A. Wares, T. Maeda, S. Kawauchi, S. Sato, M. Sato, Y. Aizu, Agarose-based tissue mimicking optical phantoms for diffuse reflectance spectroscopy, J. Vis. Exp. 138 (2018), e57578.
[16] F. Ayers, A. Grant, D. Kuo, D.J. Cuccia, A.J. Durkin, Fabrication and characterization of silicone-based tissue phantoms with tunable optical properties in the visible and near infrared domain, in: Proc. Design and Performance Validation of Phantoms Used in Conjunction with Optical Measurements of Tissue, SPIE, San Jose, CA USA, 2008.
[17] H. Jang, T.J. Pfefer, Y. Chen, Solid hemoglobin-polymer phantoms for evaluation of biophotonic systems, Opt. Lett. 40 (18) (2015) 4321–4324.
[18] T. Moffitt, Y.C. Chen, S.A. Prahl, Preparation and characterization of polyurethane optical phantoms, J. Biomed. Optic. 11 (4) (2006), 041103.
[19] S. Kleiser, D. Ostojic, B. Andresen, N. Nasseri, H. Isler, F. Scholkmann, T. Karen, G. Greisen, M. Wolf, Comparison of tissue oximeters on a liquid phantom with adjustable optical properties: an extension, Biomed. Optic Express 9 (1) (2018) 86–101.
[20] E.L. Madsen, G.R. Frank, F. Dong, Liquid or solid ultrasonically tissue-mimicking materials with very low scatter, Ultrasound Med. Biol. 24 (4) (1998) 535–542.
[21] A. Hellerbach, V. Schuster, A. Jansen, J. Sommer, MRI phantoms – are there alternatives to agar? PloS One 8 (8) (2013), e70343.
[22] S. Sarkar, A.A. Gurjarpadhye, C.G. Rylander, M.N. Rylander, Optical properties of breast tumor phantoms containing carbon nanotubes and nanohorns, J. Biomed. Optic. 16 (5) (2011), 051304.
[23] H. Li, S. Xie, Measurement method of the refractive index of biotissue by total internal reflection, Appl. Optic. 35 (10) (1996) 1793–1795.
[24] J.L. Sandell, T.C. Zhu, A review of in-vivo optical properties of human tissues and its impact on PDT, J. Biophot. 4 (11–12) (2011) 773–787.
[25] A. Yaroslavsky, P. Schulze, I. Yaroslavsky, R. Schober, F. Ulrich, H.J. Schwarzmaier, Optical properties of selected native and coagulated human brain tissues in vitro in the visible and near infrared spectral range, Phys. Med. Biol. 47 (2002) 2059–2073.
[26] T.J. Beck, W. Beyer, T. Pongratz, W. Stummer, R. Waidelich, H. Stepp, S. Wagner, R. Baumgartner, Clinical determination of tissue optical properties in vivo by spatially resolved reflectance measurements Photon Migration and, Diffuse-Light Imag. 5138 (2003) 96–105.
[27] J.F. Beek, H.J. Staveren, P. Posthumus, H.J.C.M. Sterenborg, M.J.C. Gemert, The optical properties of lung as a function of respiration, Phys. Med. Biol. 42 (1997) 2263–2272.
[28] M.S. Durkee, L.D. Nash, F. Nooshabadi, J.D. Cirillo, D.J. Maitland, K.C. Maitland, Fabrication and characterization of optical tissue phantoms containing macrostructure, J. Vis. Exp. 132 (2018), e57031.
[29] R.M. Souza, T.Q. Santos, D.P. Oliveira, R.M. Souza, A.V. Alvarenga, R.P.B. Costa-Felix, Standard operating procedure to prepare agar phantoms, J. Phys. Conf. 733 (2016), 012044.
[30] J. Cho, B. Prasad, J.K. Kim, Near-infrared laser irradiation of a multilayer agar-gel tissue phantom to induce thermal effect of traditional moxibustion, J. Innovat. Opt. Health Sci. 11 (6) (2018) 1850033.
[31] M.N. Lizuka, M.D. Sherar, I.A. Vitkin, Optical phantom materials for near infrared laser photocoagulation studies, Laser Surg. Med. 25 (2) (1999) 159–169.
[32] Oregon Medical Laser Center (OMLC), Optical Phantoms, 2017. https://www.omlc.org/classroom/phantom/. (Accessed 28 May 2019).
[33] H.-J. Schwarzmaier, A.N. Yaroslavsky, I.V. Yaroslavsky, T. Goldbach, T. Kahn, F. Ulrich, R. Schober, Optical properties of native and coagulated human brain structures, in: Proceedings of the SPIE 2970, Lasers in Surgery: Advanced Characterization, Therapeutics, and Systems, 1997.
[34] C.C. Hull, N.C. Croft, Determination of the total attenuation coefficient for six contact lens materials using the Beer-Lambert law, Ophthalmic Physiol. Optic. 16 (1996) 150–157.
[35] M. Lualdi, A. Colombo, B. Farina, S. Tomatis, R. Marchesini, A phantom with tissue-like optical properties in the visible and near infrared for use in photomedicine, Laser Surg. Med. 28 (3) (2001) 237–243.